Volume 5, Issue 1, 2015, 910-915 ISSN 2069-5837

Biointerface Research in Applied Chemistry

www.BiointerfaceResearch.com

Original Research Article Open Access Journal

Received: 21.11.2014 / Revised: 20.01.2015 / Accepted: 12.02.2015 / Published on-line: 15.02.2015

Magnetic water-soluble rhamnose-coated $Mn_{1-X}Co_XFe_2O_4$ nanoparticles as potential heating agents for hyperthermia

Sarah Briceño [1,*], Pedro Silva [1], Werner Bramer-Escamilla [1], José Zabala [1], Olgi Alcala [1], Yannick Guari [2], Joulia Larionova [2], Jerome Long [2]

[1]Laboratorio de Física de la Materia Condensada, Centro de Física, Instituto Venezolano de Investigaciones Científicas (IVIC), Apartado 20632, Caracas 1020-A, Venezuela

[2]Institut Charles Gerhardt Montpellier, UMR 5253 CNRS-UM2, Chimie Moleculaire et Organisation du Solide, Universit Montpellier II, Place E. Bataillon, 34095 Montpellier Cedex 5, France

*corresponding author e-mail address: ***sbriceno@ivic.gob.ve***

ABSTRACT

Water-soluble rhamnose-coated mixed manganese-cobalt ferrite nanoparticles $Mn_{1-X}Co_XFe_2O_4$ ($0 \leq x \leq 1$) specifically designed as magnetic fluid hyperthermia heat mediators were successfully synthesized by thermal decomposition of molecular precursors in a size range between 6 - 12 nm. The formation of the nanoparticles (NPs) and modification of their surface with a rhamnose derivative were confirmed by FTIR spectroscopy, X-ray diffraction (XRD) and transmission electronic microscopy (TEM). Electron Paramagnetic Resonance (EPR) was used to study the temperature dependence of the magnetic behavior of the samples coated with rhamnose. The magnetic properties being investigated at 2.5 and 300 K include blocking temperature (T_B), saturation magnetization (M_s), remnant magnetization (M_R) and coercive field (Hc). The magnetic properties carried out at 300 K show the increase of the saturation magnetization (M_s) at the Mn^{2+} ratio x = 0.75. The variation of SAR and magnetization of $Mn_{1-X}Co_XFe_2O_4$ with Mn^{2+} ratio shows similar dependence. The advantage of the designed rhamnose-coated $Mn_{1-X}Co_XFe_2O_4$ system lies in the fact that versatile combinations of Mn^{2+} and Co^{2+} components can facilitate the tuning of the magnetic properties to optimize the Specific Absorption Rate (SAR).

Keywords: ferrite, nanoparticles, hyperthermia, specific absorption rate.

1. INTRODUCTION

Magnetic nanoparticles (NPs) have received great deal of attention due to their biomedical applications such as drug delivery and hyperthermia treatment for cancer, referring to the introduction of ferromagnetic or superparamagnetic particles into the tumor tissues [1]. For magnetic hyperthermia, the magnetic nanoprobes should be biocompatible and evenly suspended in water based fluids. Furthermore, the particles should not precipitate due to gravitational or electrostatic forces in order to avoid embolic problems. To shorten treatment time and minimize discomfort from prolonged heating, the nanoparticles should heat rapidly. To accomplish this, the Specific Absorption Rate (SAR), which is the heating power of a magnetic material per gram, of the nanoparticles should be maximized. The heating effect and thus the efficiency of the NPs as hyperthermia agent, depends on the NPs composition, size and shape as well as the frequency and amplitude of the applied alternating magnetic field [2]. Recent studies have demonstrated that iron oxide NPs are very promising candidates due to their biocompatibility, relative non toxicity and easy surface modification [3]. In order to achieve more safety for biomedical applications, avoid the phagocytosis problems and blood circulation for a relatively long period of time, iron oxide NPs must be covered by a biocompatible organic or inorganic coating. In this line of thought, numerous iron-oxide based systems with different biocompatible stabilizing ligands have been proposed as efficient heat mediators. Recently, some of us reported on the synthesis, characterizations, magnetic, relaxometric and hyperthermia properties of a series of magnetite (Fe_3O_4) NPs with different sizes ranging from 4 to 35 nm coated with sugar derivatives containing rhamnose, mannose and ribose moieties. These NPs were prepared by the thermal decomposition of iron containing molecular precursors and then coated with specially prepared organic ligands bearing a phosphonate group on one side and sugar moieties on the other side. In this way a strong anchorage of the organic ligand on the organic surface was simply realized by ligand exchange, due to covalent bonding between Fe^{3+} atom and the phosphonate group. Sugars were chosen in order to offer biocompatibility, and targeting because these carbohydrates in particular rhamnose, which is a substrate of skin lectin may selectively target skin cancer cells. These magnetite-based NPs of 16-18 nm were found to represent an efficient bi-functional targeting system for theranostics applications, as they have very good transverse relaxivity (three times larger than the best currently available commercial products) and a large heat release upon application of radio frequency (RF) electromagnetic radiation with amplitude and frequency close to the human tolerance limit. These promising results encouraged us to pursue our effort in the synthesis of magnetic NPs to extend our effort toward nano-objects of different composition. By adding other ions such as Ni^{2+}, Mn^{2+} and Co^{2+} to iron oxide NPs, a range of ferrites nanoparticles with improved magnetic properties can be

obtained. For instance, this flexibility can be used to tune the NPs magnetic moment, magnetization, the magnetocrystalline anisotropy and coercivity and thus the heating power of materials for hyperthermia applications by creating cubic mixed-ferrite materials. In this series, nano-sized manganese doped cobalt ferrites are promising nanomaterials for biomedical applications and, in particular for theranostics science (combining therapy and diagnosis) because they combine high magnetization values of Mn^{2+} with the important anisotropy coming from the presence of Co^{2+} ion, which should tune the magnetic properties resulting in appearance of high relaxivity and high heating capacity. In this paper we report on the synthesis, structural, magnetic properties and heat generation capabilities $Mn_{1-X}Co_XFe_2O_4$ ($0 \leq x \leq 1$) NPs NPs coated with a rhamnose derivative. These NPs are perfectly dispersible in water and present sizes ranging from 6 – 12 nm.

2. EXPERIMENTAL SECTION

The syntheses were carried out using standard airless procedures and commercially available reagents. Absolute ethanol, hexane, methanol, and dichloromethane (99%) were used as received. The Tetrahydrofurane, THF, was purified by distillation over sodium m. 1,2-hexadecanediol (90%), oleic acid (90%), ammonia 2.0M solution in methanol. Phenyl ether (99%), oleylamine approximate C18 content (97%), iron(III) acetylacetonate (99+%) were purchased from Acros Organics. Rhamnose was purchased from Benn Chemicals. $Mn_{1-X}Co_XFe_2O_4$ ($0 \leq x \leq 1$) ferrite NPs coated with oleic acid was synthesized by the thermal decomposition method. The experimental setup consisted of a system reflux under Ar atmosphere using a 250 mL condenser and heating mantle. The typical procedure consisted of mixing 2 mmol $Fe(acac)_3$, 0.5 mmol $Mn(acac)_3$, 0.5 mmol $Co(acac)_3$, 5.0g 1,2 hexadecanediol, 1.0 ml oleic acid, 1.0 ml oleylamine and 30 ml benzyl ether. The nuclei formation and the growth of the Nps were obtained when temperature was increased to 200 °C for 30 min with a blanket of argon and heated to reflux at 265 °C for another 30 min. The black-brown mixture was cooled to room temperature by removing the heat source. Under ambient conditions, ethanol was added to the mixture, and a black material was precipitated and separated via centrifugation [4] and finally stabilized by oleic acid/oleylamine in hexane. The second step consists in replacing the oleic acid/oleylamine by the rhamnose [5, 6]. The ligand exchange reaction was realized at reflux in tetrahydrofuran (THF) for 24h and them removing the acetate group from the -OH of the carbohydrate into methanol/ammonia 2M to obtain RH-$Mn_{1-X}Co_XFe_2O_4$. The nanoparticles become soluble in water and the solutions are stable for several months. Phase identification, purity, relative crystallinity and structure of the samples were determined at room temperature using a PanAnalytical difractometer Bruker D8 Advance diffractometer equipped with Cu Kα radiation and operating in θ–2θ Bragg Brentano geometry at 40kV and 40mA. The modification of the surface of the NPs was confirmed using a FTIR Perkin Elmer 1600 spectrometer. Size and morphology of products were tested with a transmission electron JEOL 1200EXII microscope operated at 100 kV. Magnetic characterization was made in a homemade vibrating sample magnetometer at 300K. EPR measurements were carried out in a BRUKER EMX spectrometer. The heat generation capabilities were measured at 473 kHz and 11 mT using a MagneTherm system from nanoTherics.

3. RESULTS SECTION

The modification of the NPs surface was confirmed by FTIR spectroscopy in the 400 - 4000 cm^{-1} range.

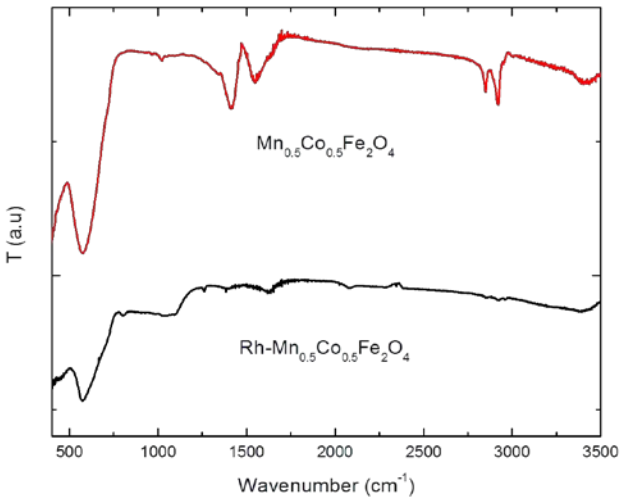

Figure 1. FTIR spectra of $Mn_{0.5}Co_{0.5}Fe_2O_4$ and RH-$Mn_{0.5}Co_{0.5}Fe_2O_4$.

Figure 1 exhibits the FTIR spectra of $Mn_{0.5}Co_{0.5}Fe_2O_4$ coated with oleic acid/ oleylamine and the rhamnose-coated RH-$Mn_{0.5}Co_{0.5}Fe_2O_4$ NPs as representative samples of the system $Mn_{1-X}Co_XFe_2O_4$. In the IR spectra of $Mn_{0.5}Co_{0.5}Fe_2O_4$ we observe two characteristics bands at 2926 and 2855 cm^{-1} that corresponds with the asymmetric and symmetric stretching of C-H bonds of the aliphatic chain. In the IR spectra of RH-$Mn_{0.5}Co_{0.5}Fe_2O_4$ the carbohydrate fingerprint was observed at 1072 cm^{-1} assigned to C-O-C demonstrate the removing of oleic acid replaced by the rhamnose and the C-H bonds of the aliphatic chain almost completely disappears. The characteristic metal-oxygen band is observed in the IR spectra of spinel structure at 571 cm^{-1}, and corresponds to intrinsic stretching vibrations of the metal at the tetrahedral site.

The obtained NPs were investigated by Transmission Electronic Microscopy (TEM) in order to obtain information about the shape and size of the samples. Figure 2 demonstrates the presence of the morphology like spheres for a series of representative samples for $MnFe_2O_4$, $Mn_{0.5}Co_{0.5}Fe_2O_4$ and $CoFe_2O_4$ and after rhamnose anchoring. The size distribution of the NPs ranges from 6 to 12 nm. The size distributions obtained from TEM show that the mean size of the NPs stabilized by oleic acid/oleylamine in hexane and the NPs cover with rhamnose are identical, indicating that the nature of sugar does not influence the size and shape of the NPs.

XRD studies of $Mn_{1-X}Co_XFe_2O_4$ system have proved the formation of single phase cubic spinel with high crystalline structure for all samples. The hkl indices of the samples are [220], [311], [222], [400], [422], [511] and [440] as plotted in Figure. 3. These planes indicate the presence of a mixed type cubic spinel structure. Mixed spinel ferrites ($0 \leq x \leq 1$) were checked with XRD cards of $CoFe_2O_4$ NPs. (JCPDS file: 22-1086) and $MnFe_2O_4$ (JCPDS file: 74-2403) [12]. No other impurity phases are observed.

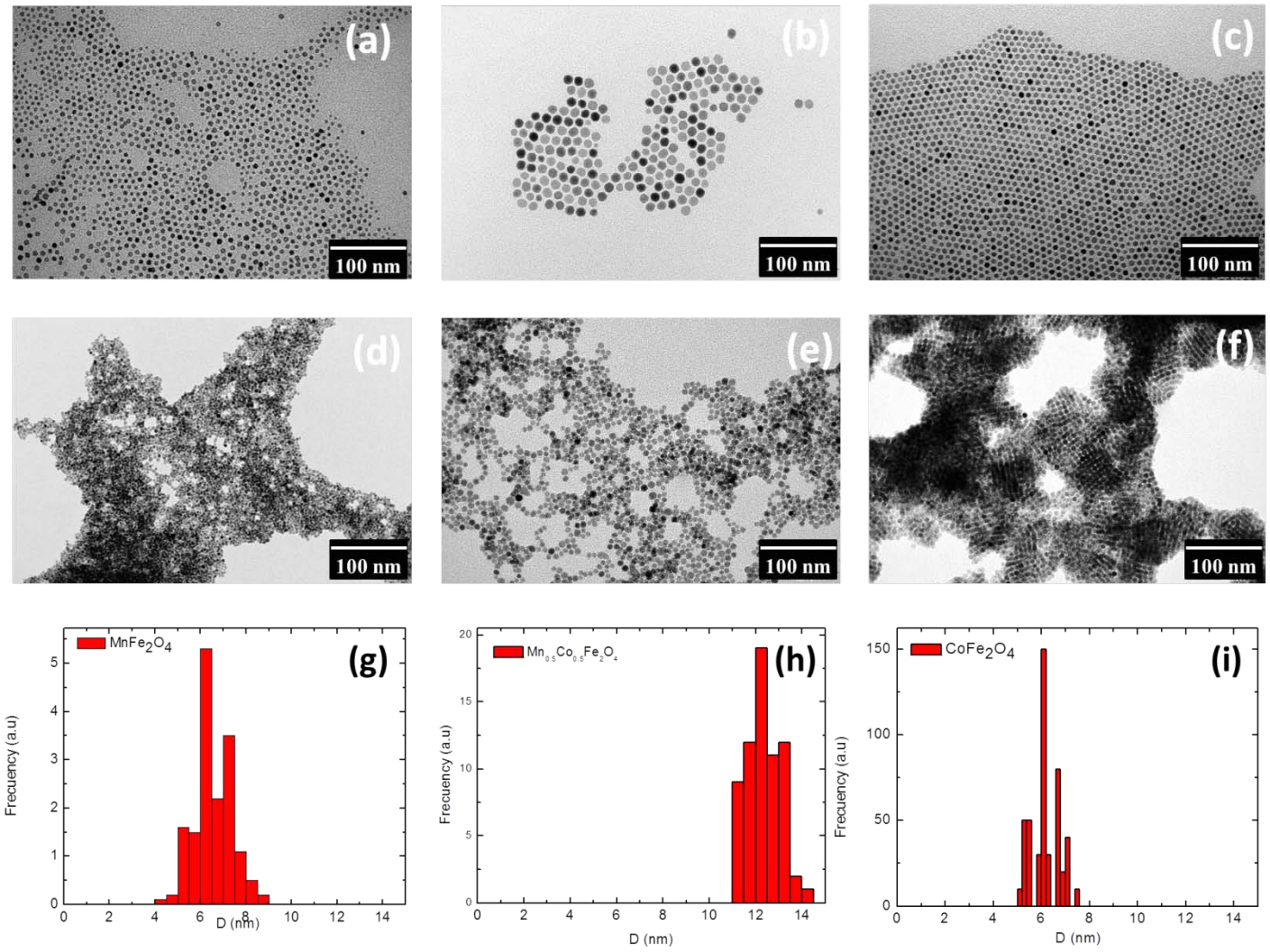

Figure 2. TEM images of (a) $MnFe_2O_4$, (b) $Mn_{0.5}Co_{0.5}Fe_2O_4$, (c) $CoFe_2O_4$, (d) RH-$MnFe_2O_4$, (e) RH-$Mn_{0.5}Co_{0.5}Fe_2O_4$, (f) RH-$CoFe_2O_4$ and size distribution histograms of (g) $MnFe_2O_4$, (h) $Mn_{0.5}Co_{0.5}Fe_2O_4$ and (i) $CoFe_2O_4$ nanoparticles.

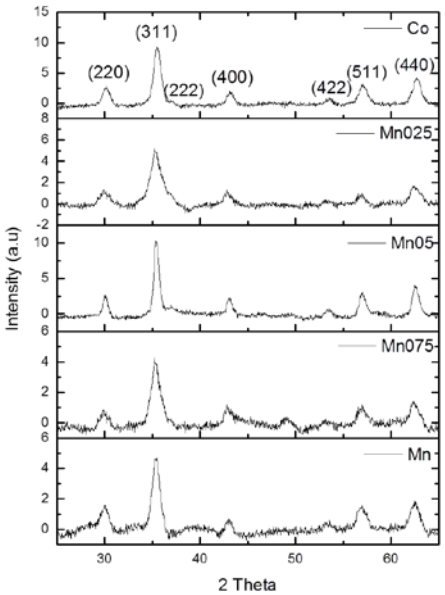

Figure 3. XRD patterns of $Mn_{1-X}Co_XFe_2O_4$ ($0 \leq x \leq 1$).

Magnetic properties of ferrites are directly related to the chemical composition and distribution of the cations over tetrahedral and octahedral lattice sites. Spinel type compounds generally behave as ferrimagnets, so the magnetizations of them M(x) are the net moments of A and B sites, and given by

$$M(x) = M_{B(x)} + M_{A(x)} \qquad (1)$$

where, M_B and M_A are the magnetic moments of B and A sites, respectively. According to the capability sequence for the cations to occupy the B sites, $Mn^{2+} > Co^{2+} > Fe^{2+}$, the cation distribution in mixed Mn-Co ferrospinel having the formula $Mn_{1-X}Co_XFe_2O_4$ can be expressed as:

$$Fe^{3+}_{1-a-b}\, Co^{2+}_{a}\, Mn^{2+}_{b}\, (Co^{2+}_{x-a} Mn^{2+}_{1-a-b} Fe^{3+}_{1+a+b}) \qquad (2)$$

where x varies between 0 to 1 in the present study, while a and b are the fraction of Co^{2+} and Mn^{2+} ions.

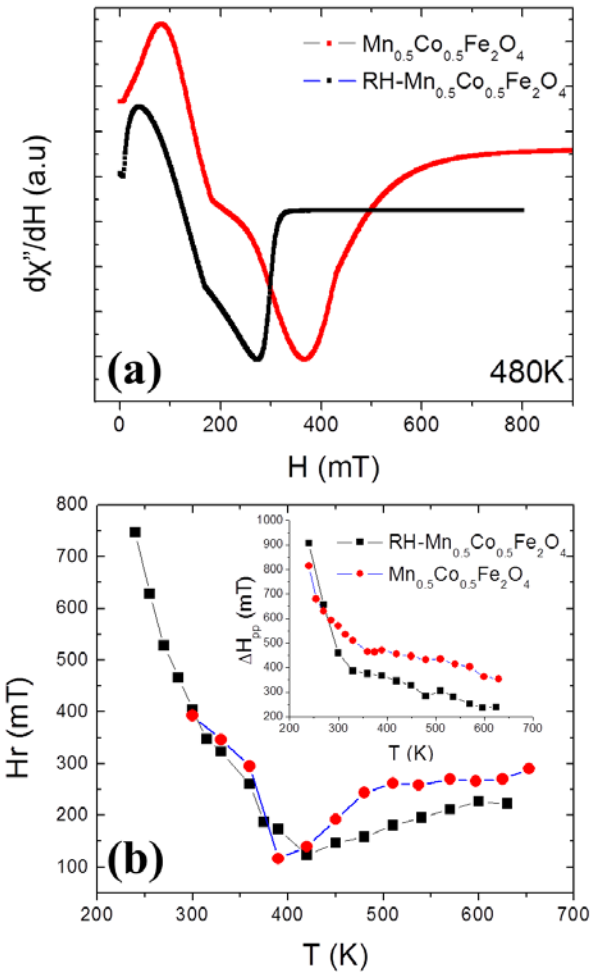

Figure 4. Unnormalized EPR spectra at 480 K and resonant field (H_R) temperature dependence parameters of $Mn_{0.5}Co_{0.5}Fe_2O_4$ and RH-$Mn_{0.5}Co_{0.5}Fe_2O_4$.

Figure 4 (a) shows the unnormalized electron magnetic resonance EPR spectra at T = 480 K for the samples $Mn_{0.5}Co_{0.5}Fe_2O_4$ and RH-$Mn_{0.5}Co_{0.5}Fe_2O_4$. A well-defined spectrum is observed, that could consist of a superposition of a narrow and broad component or even a sum of different contributions originated from the small size dispersion in the samples. Figure 4 (b) demonstrates the temperature dependence of the resonant field (H_R) for the samples studied in the range from 200 to 650 K. When the temperature is decreases from T = 650 K H_R for the sample RH-$Mn_{0.5}Co_{0.5}Fe_2O_4$ remains approximately constant until T = 480 K; below this temperature H_R quickly decreases probably due to the strong zero field absorption present in the sample. The inset of Figure 4 (b) shows the linewidth behavior as a function of temperature showing a continuous increment, probably due to an increment of the dipolar interaction of the NPs [8]. The behavior for sample $Mn_{0.5}Co_{0.5}Fe_2O_4$ stabilized with oleic acid/oleylamine is similar to sample covered with rhamnose. H_R decrease smoothly when the temperature decreased to 390 K, the linewidth increases very quickly when the temperature decreased. This type of thermal behavior has been frequently observed in the EPR spectra of the iron oxide NPs ensembles, signifying the gradual suppression of the averaging effect of thermal fluctuations or the emergence of spin-glass freezing with temperature lowering [10]. Bellow 400 K the H_R increment in both samples. This behavior can be explained with by formation of field-induced agglomerates when applying an external magnetic field causing the demagnetization factor to decrease [9]. A similar behavior is expected as a function the temperature due to the formation of agglomerates as we can see in the Figure 3.

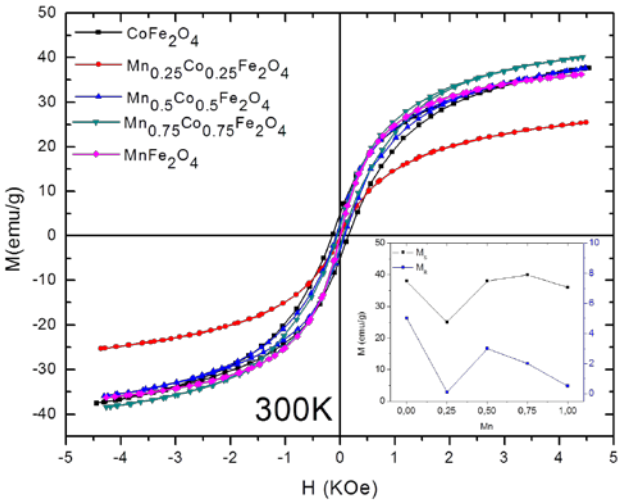

Figure 5. Magnetization versus applied field at 300 K and in the inset, saturation magnetization (Ms) and remanent magnetization (Mr) as a function of the Mn^{2+}.

Figure 5 displays the field dependent magnetization curves obtained for the system $Mn_{1-X}Co_XFe_2O_4$ at 300 K. The hysteresis loops display nonzero coercivity and remnant magnetization, confirming that it is largely blocked at room temperature. This is demonstrated by the small magnetic nanoparticles dimensions that result from XRD and TEM analysis. The values of the magnetic properties are given in Table 1. Saturation magnetization values (Ms) range from 25 up to 40 emu/g. As shown in the inset of the Figure 5 the Ms had a strong dependence on the Mn^{2+} ratio. Particularly, the $Mn_{0.75}Co_{0.25}Fe_2O_4$ NPs had the highest Ms value of 40 emu/g. The increase in Ms by increasing the Mn^{2+} ratio up to x = 0.75 is thought to be due to the increase in magnetic moment of the unit cell up to 7.5 μB which resulted from the replacement of the Co^{2+} by the Mn^{2+} ions on the A-site [3, 13].

Table 1. Average particle size, magnetic properties and Specic Absorption Rate (SAR) of RH-$Mn_{1-X}Co_XFe_2O_4$.

Sample	Size (nm)	T_B (K)	M_S (emu/g)	M_R (emu/g)	Hc (Oe)	SAR (W/g)
$CoFe_2O_4$	6 ± 2	300	38	5.11	0.15	10
$Mn_{0.25}Co_{0.75}Fe_2O_4$	7 ± 2	208	25	-	0.004	5
$Mn_{0.5}Co_{0.50}Fe_2O_4$	12 ± 2	300	37	2.97	0.078	14
$Mn_{0.75}Co_{0.25}Fe_2O_4$	8 ± 2	148	40	2.46	0.050	8
$MnFe_2O_4$	6 ± 2	70	36	0.28	0.062	0

Zero-field-cooled (ZFC) magnetizations were measured by cooling the $Mn_{1-X}Co_XFe_2O_4$ samples in a zero magnetic field and then increasing the temperature in a static field of 50 Oe, while field-cooled (FC) curves were obtained by cooling the samples in the same static field (Figure 6). Blocking temperatures values (T_B) of the samples ($0 \leq x \leq 0.5$) are found to decrease considerably as manganese content increases, which may be related to the lowering of the inter-sublattice exchange coupling between A and B sublattices. The low blocking temperature (70K) in the sample x = 0 relates with the superparamagnetic nature of the manganese

ferrite. On the contrary, the ZFC of the samples with x = 0.5 and x = 1 increases continuously as the temperature increases and never reaches a maximum, suggesting the presence of a ferromagnetic like behavior at room temperature. The large cusps in the M-T curves have also been observed for similar systems which were attributed to the interaction between the NPs in the samples or grain growth effect as the samples were heated at high temperatures [12].

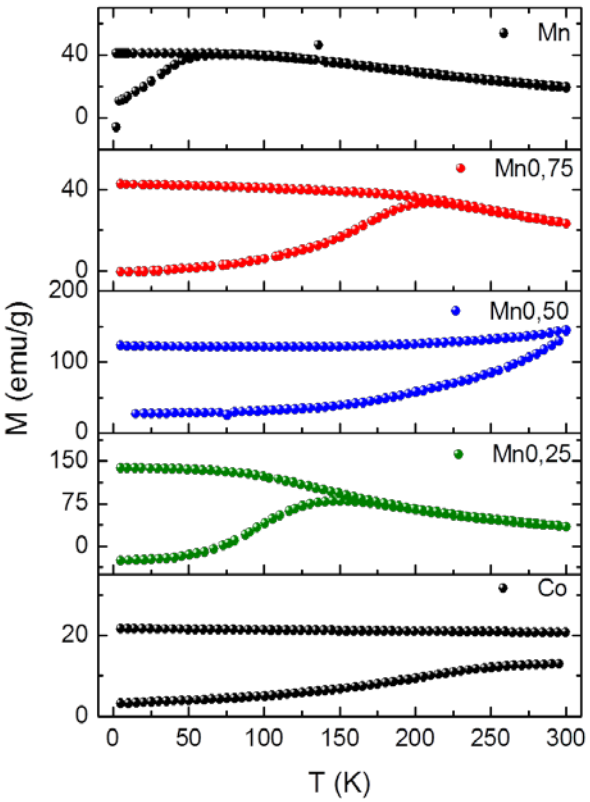

Figure 6. Magnetization versus temperature plots FC/ZFC of $Mn_{1-X}Co_XFe_2O_4$.

Heat dissipation of the system $Mn_{1-X}Co_XFe_2O_4$ produced by the delay in the relaxation of the magnetic moment may be observed when the NPs are exposed to an alternating magnetic field of proper frequency. The dependence of the heat dissipation was measured at 473 kHz and at 11 mT. The Specific Absorption Rate (SAR) in units of Watts per gram (W/g) was calculated to compare the efficiency of heating each sample using the Newton's model, given by:

$$T(t) = T_\infty + (T_0 - T_\infty)e^{-\left(\frac{t}{\tau}\right)} \quad (3)$$

T_∞ : Saturation temperature.
T_0: Initial temperature.
τ: Relaxation time.

Relaxation time τ allows a relationship with the saturation temperature, which is:

$$T(\tau) = (0.632).T_\infty \quad (4)$$

In this way we obtain the temperature on the relaxation time of the system which represents approximately 63.2% of the saturation temperature according to (4). Furthermore, the ability of an energy absorbing system can be studied using the SAR (Specific Absorption Rate), which is defined as the rate of increase in time and per unit mass of a sample that has been subjected to a temperature change [11]. Its definition is:

$$SAR = C_m \frac{\Delta T}{\Delta t} \quad (5)$$

C_m: Specific heat of the sample.
ΔT: Temperature increase from its initial value.
Δt: Time increment where the temperature variation of the system occurred.

The disadvantage of this definition of SAR lies in the fact that its value depends on the initial and final points taken to calculate the increase of temperature and time, so that the value that depends on these points is arbitrary and makes comparisons difficult when increase ranges are not the same. Therefore, in this paper we propose an alternative way to calculate the SAR based relaxation time τ obtained using (3):

$$SAR = \frac{\Delta T(\tau,T_0)}{\Delta \tau} = \frac{T(\tau)-T_0}{\tau - t_0} \quad (6)$$

$T(\tau)$: Temperature of the system evaluated at the relaxation time.
T_0: Initial temperature of the system.
τ: Relaxation time of the system.
t_0: start time for the initial temperature of the system.

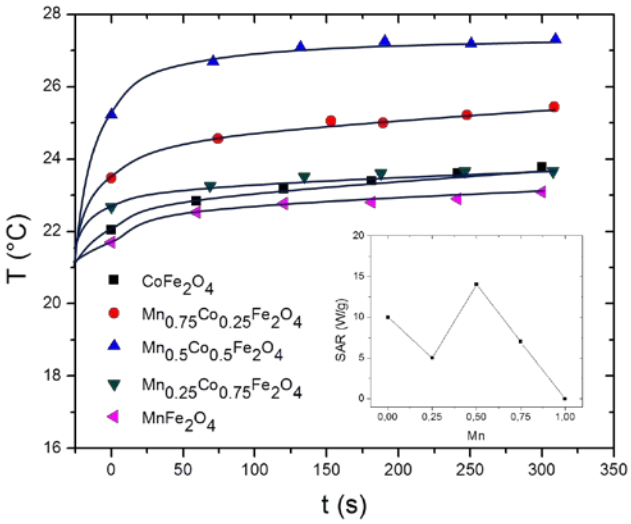

Figure 7. Time evolution of temperatures of $Mn_{1-X}Co_XFe_2O_4$ and in the inset the Specific Absorption Rate (SAR) as a function of the Mn^{2+} content.

The temperatures versus time curves describing the heating process of $Mn_{1-X}Co_XFe_2O_4$ are shown in Figure. 7. The initial slope of the temperature versus time was obtained from these curves and used to determine the SAR values. The inset in the Figure 7 reports the measured SAR values as a function of the Mn^{2+} content. The highest 13.88 W/g SAR value is recorded for $Mn_{0.5}Co_{0.5}Fe_2O_4$. The study confirmed that the specific absorption rate values depend on the average size, chemical formula and cation distribution. The key advantage of the $Mn_{1-X}Co_XFe_2O_4$ system lies in the fact that versatile combinations of Co^{2+} and Mn^{2+} ratio can bring facile tuning of the magnetic properties. For example, when $Mn_{0.5}Co_{0.5}Fe_2O_4$ NPs with high Ms (40 emu/g) were used, SAR was (13.88 W/g). This is 4.5 times higher than that for conventional iron-oxide magnetic nanoparticle (3 W/g) [6].

4. CONCLUSIONS

A series of water-soluble rhamnose-coated $Mn_{1-X}Co_XFe_2O_4$ NPs have successfully been prepared by thermal decomposition of molecular precursors and post-synthetic sugar coating. The structural and textural characterizations have revealed that $Mn_{1-X}Co_XFe_2O_4$ have a single spinel structure with sizes ranging between 6 and 12 nm. The highest value of specific absorption rate (SAR) obtained for $Mn_{0.5}Co_{0.5}Fe_2O_4$ NPs is 13.88 W/g. The magnetic field applied in these cases is 11mT, which is situated within the acceptable range limitations imposed by the potential use for the human body. We take advantage of the different contributions of Mn^{2+} and Co^{2+} in the $Mn_{1-X}Co_XFe_2O_4$ ferrites to tune the magnetic properties and maximize the SAR, which is a challenge of the conversion efficiency. The optimized samples have SAR values that are in the order of magnitude than conventional iron oxide NPs.

5. REFERENCES

[1] Ang K.L., Venkatraman S., Ramanujan R.V., Magnetic PNIPA hydrogels for hyperthermia applications in cancer therapy, *J. Mat. Sci. Eng*. C27, 347, **2007**.

[2] Baker I., Zeng Q., Li W., *et al*., Heat Deposition in Iron Oxide and Iron Nanoparticles for Localized Hyperthermia, *J. Appl. Phys*. 99, 08H106, **2006**.

[3] Sharifi I., *et al.*, Ferrite-based magnetic nanofluids used in hyperthermia applications, *J. Magn. Magn. Mater.* 324, 903-915, **2012**.

[4] Sun S., Zeng H., *et al*., Monodisperse MFe2O4 (M = Fe, Co, Mn) Nanoparticles, *J. Am. Chem. Soc.* 126, 273, **2004**.

[5] Lartigue L., Oumzil K., Guari Y., *et al*., Water-Soluble Rhamnose-Coated Fe3O4 Nanoparticles, *Org. Lett*., 11, 14, 2992-2995, **2009**.

[6] Lartigue L., Innocenti C., Kalaivani T., *et al*., Water-Dispersible Sugar-Coated Iron Oxide Nanoparticles. An Evaluation of their Relaxometric and Magnetic Hyperthermia Properties, *J. Am. Chem. Soc.* 133, 10459-10472, **2011**.

[7] Zhou B., *et al*., Magnetism and phase transition for CoFe2−xMnxO4 nanocrystalline thin films and powders, *J. Magn. Magn. Mater*., 247, 70-76, **2002**.

[8] Silva P., *et al*., Temperature dependence of the EPR spectra for the Ni1−xCoxFe2O4 nanoparticles, *J Phys Conf.*, 200, 082023, **2010**.

[9] Goncalves G.R.R., *et al*., Magnetic resonance investigation of the particle–particle equilibrium distance within small agglomerates in magnetic fluids, *J. Magn. Magn. Mater*. 289, 142-145, **2005**.

[10] Guskos N., *et al*., FMR study of magnetic nanoparticles embedded in non-magnetic matrix, *J. Achievem. Mat. Manuf. Eng*. 24 (1), 26-35, **2007**.

[11] Ma M., *et al*., Size dependence of specific power absorption of Fe3O4 particles in AC magnetic field, *J. Magn. Magn. Mater*., 268, 33-39, **2004**.

[12] Lee J.H., Jang J.T., *et al*., Exchange-coupled magnetic nanoparticles for efficient heat induction, Nat. Nanotechnol. 6, 418-422, **2011**.

[13] Jeun M., Moon S.J., Kobayashi H., *et al*., Effects of Mn concentration on the ac magnetically induced heating characteristics of superparamagnetic $Mn_xZn_1{-}xFe_2O_4$ nanoparticles for hyperthermia, *Appl. Phys. Lett.* 96, 202511, **2010**.

6. ACKNOWLEDGEMENTS

We thank MPPCTI - ECOS-Nord (V13PS01), CNRS, University of Montpellier and the Instituto Venezolano de Investigaciones Cientificas for financial support. The authors thank Mmes D. Granier and C. Rebeil (PAC Balard, University of Montpellier) for XRD and magnetic measurements, respectively.